A NOVEL SOURCE LOCALIZATION SCHEME BASED ON UNITARY ESPRIT AND CITY ELECTRONIC MAPS IN URBAN ENVIRONMENTS

H. B. Song, H. G. Wang, K. Hong, and L. Wang

The Electromagnetics Academy at Zhejiang University
Zhejiang University
Hangzhou 310027, China

Abstract—In this paper, a novel source localization scheme is proposed based on the unitary ESPRIT algorithm with back ray tracing technique and the city electronic maps. Our scheme can be summarized into two steps. First, the unitary ESPRIT algorithm is employed to estimate the angles and delays of the arrival rays radiated from the source. Second, based on the obtained information we devise a back ray tracing technique to recover the signal propagation paths according to the Geometrical Theory of Reflections and the city electronic map. After these two steps the source position can be obtained by averaging all the estimated positions. In order to minimize estimated errors caused by the Unitary ESPRIT, a valid-range selection criterion for the judgment of the validity of the estimated position data is proposed. On the other hand, we introduce a path length weighting factor to reduce the estimated errors caused by the terrain data inaccuracy. This position method can locate both the line of sight (LOS) and non-line of sight (NLOS) sources efficiently and it also can locate multi-sources simultaneously. Six simulations are carried out in three terrain scenarios. The numerical results demonstrate that our model can be applied to estimate the positions for both 2D and 3D cases. The accuracy of our model for a cell of $80\,\text{m} \times 45\,\text{m}$ can reach $10\,\text{m}$ when SNR is greater than $10\,\text{dB}$.

1. INTRODUCTION

Recently, source localization becomes an ad hoc topic in wireless communications. There are many typical methods [1–5] for locating a source, e.g., time-of-arrival (TOA) [6, 7], time difference of arrival

---

Corresponding author: H. G. Wang (hgwang@zju.edu.cn).

Table 1. Comparison between different position methods (symbol $\sqrt{}$ denotes the corresponding parameter is used).

		ToA	DoA	TDoA	RSS	As	Performance	Description
Trilateration	[4][6][7]	√					Only for LoS source	Trilaterating with signal parameters of LoS paths
	[8][9][10]		√					
	[3][5][32]			√				
	[1][2]		√		√			
	[11]	√	√					
	[12]		√	√				
Fingerprint	[33][34]			√	√		For both LoS and NLoS source	Database correlation method
	[16][17]		√			√		
Our method		√	√				For both LoS and NLoS source	Back ray tracing with ToA and DoA

(TDoA) [32], angle-of-arrival (AOA/DOA) [8–10] approach and some hybrid techniques [11, 12] as shown in Table 1. Most of these methods are based on trilateration utilizing ToA, DoA, TDoA, RSS and the diverse combinations of these parameters. The TOA and AOA approaches need more than one base station and the estimation accuracy is low for non-line of sight (NLOS) sources. Although various NLOS mitigation techniques [7, 13–15] have been proposed to improve the location accuracy, these techniques require that the number of available LOS base stations is greater than that of the NLOS base stations. In [11] a hybrid TOA/AOA positioning algorithm was proposed. Four different statistical propagation environments models, i.e., bad urban, urban, suburban, and rural, were conducted in [11]. However, it does not consider the real propagation environments. All trilateration methods mentioned above have the same weak point, i.e., all of them perform well for LoS cases, but badly for NLoS cases. Recently, a new method called fingerprint method show better performance than the trilateration. In this method, the source is located by comparing measured parameters, such as DoA TDoA ToA and RSS, to the pre-measured reference data [33, 34]. However, it needs an accurate database for storing these pre-measured data and thus becomes unrealistic for the dynamic outdoor radio environments. A modified version was proposed in [16, 17] that determines source positions by comparing the spatial characteristics estimated from data measurements to that obtained from ray tracing analysis with terrain data. Though this modified method does not need to establish the pre-measured reference database, it increases the computation burden.

Unlike the methods mentioned above, a novel localization method

is proposed in this paper. It employs the Back Ray Tracing (BRT) [19, 20] technique with the city electronic map and high resolution signal parameter estimation algorithm-Unitary ESPRIT (UESPRIT) [21, 22].

UESPRIT is a simple and highly efficient method for estimating signal parameters based on the translational invariance geometry of an array. It has been proved that UESPRIT can gain higher accuracy in signal subspace estimations compared with MUSIC and ESPRIT [21, 22]. In recent years, it has been extended to the solutions of multidimensional cases. In our paper we use it to estimate the direction of arrival (DoA) and time of arrival (ToA).

With the estimated DoA and ToA using UESPRIT, the arrival angles and the lengths of the paths of the signals can be obtained. According to these angles, the BRT emits signals from the receiver. Then the transmitting waves will move forward, hit the building, and be reflected. They will not stop until the lengths of the paths reach the estimated ones. The stop positions are the locations of the sources. The final estimated position of the source is determined by averaging all the estimated positions according to each path traced by the BRT.

For the case the transmitting waves hit around the corner of the building, the estimated position may be far away from the actual one, when the estimated DoA and TDoA deviate a little from the real DoA and ToA. To minimize the estimated errors, a valid range selection criterion for the judgment of the validity of the estimated position data is employed in this paper. After eliminating the invalid estimated positions using this criterion, the average of those valid estimated positions will be made, which is the ultimately estimated source location.

Usually, the geometry data of the terrain is inaccurate. Our research in part 3 of Section 4 discovers that the estimated error caused by this inaccuracy is correlated with the number of inaccurate walls that the signal has passed and the errors of the walls. From the statistical point of view, the number of inaccurate walls that the signal has passed is proportional to the path length. So, instead of averaging of the valid estimated positions, we devise a path length weighting factor to each valid estimated positions, and then, determine the final estimated position by weighted plus of all the valid estimated positions.

Six simulations results demonstrate that our model can be applied to estimate the positions for both 2D and 3D cases. The accuracy of our model for a cell of $80\,m \times 45\,m$ can reach $10\,m$ when SNR is greater than $10\,dB$. This method can also be extended to multi-sources location.

The organization of this paper is as follows. In the next

section, the famous UESPRIT algorithm is reviewed. The location procedure with UESPRIT and BRT technique is proposed in Section 3. Section 4 treats the location error of our method. First, the parameter estimation accuracy of UESPRIT is analyzed in Section 4.1. Second, in Section 4.2, we investigate the location error caused by UESPRIT and devise a remedy using the valid range selection criterion. In Section 4.3, the location error caused by the terrain data inaccuracy is studied and the path-length weighting factors are introduced to minimize the localization errors. In Section 4.4, we also discussed the blind region of our method. The numerical results are shown in Section 5.

2. A BRIEF REVIEW OF UESPRIT

In order to let the readers have an idea of UESPRIT, here we give a brief review of this method. UESPRIT is applicable to centro-symmetric array configurations. A sensor array is called centro-symmetric if its element locations are symmetric with respect to the centroid and the complex response patterns of paired elements are the same [23]. The uniform linear array (ULA) used in practice is centro-symmetric. The ULA is decomposed into two subarray, viz. subarray 1 and subarray 2, by selection matrices J_1 and J_2 that choose l elements of ULA, as shown in Fig. 1, where J_1 and J_2 are generally centro-symmetric with respect to one another (1),

$$J_2 = \Pi_l J_1 \Pi_L, \tag{1}$$

Π_l and Π_L are the $l \times l$ and $L \times L$ exchange matrices with ones on their antidiagonal and zeros elsewhere. L denotes the number of elements in ULA. The selection matrices J_1 and J_2 are shown in Fig. 1. If there are d different signals arrive at ULA, the measurement data matrix $X \in \mathbb{C}^{L \times 1}$ is

$$X = A_G S + n \tag{2a}$$

The vector $S = [\ S_1 \quad S_2 \quad, \ldots, \quad S_d\ ]^T$ is the corresponding d different signals, $n \in \mathbb{C}^{L \times 1}$ denotes the noise sample, and $A_G \in \mathbb{C}^{L \times d}$ is the
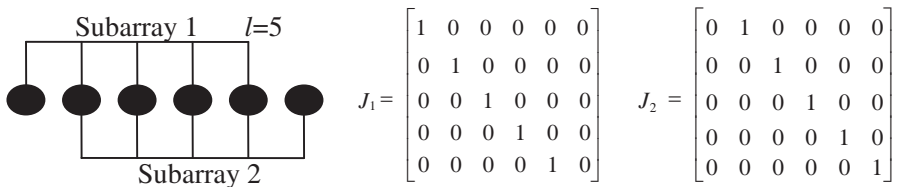
Figure 1. Subarray for ULA.

global array steering matrix, which can be written as the vandermonde matrix,

$$A_G = [a(\mu_1) \ a(\mu_2) \ \ldots \ a(\mu_d)], \tag{2b}$$

where $a(\mu_i) = [\ 1 \ \ e^{j\mu_i} \ \ e^{j2\mu_i} \ \ \ldots \ \ e^{j(L-1)\mu_i} \ ]^T$, μ_i is the signal parameter need to be estimated. It is easy to find out that (2b) satisfy the following invariance properties:

$$J_1 A_G \ \cdot \Phi = J_2 A_G \ , \tag{3}$$

where the diagonal matrix $\Phi = \text{diag}\{e^{j\mu_i}\}_{i=1}^d$. According to the paper [25], (3) can be changed to

$$K_1 D \cdot \Omega = K_2 D. \tag{4}$$

In Equation (4), D is the transformed steering matrix, which is defined as $D = Q_L^H A_G$ [16], $K_1 \ K_2$ and Ω are the transformed selection matrices and the real-valued diagonal matrices (5)

$$\begin{aligned} K_1 = 2 \cdot \text{Re} \left\{ Q_l^H J_2 Q_L \right\}, \ K_2 = 2 \cdot \text{Im} \left\{ Q_l^H J_2 Q_L \right\} \\ \text{and } \Omega = \text{diag} \left\{ \tan \left[\tfrac{\mu_i}{2} \right] \right\}_{i=1}^d, \ 1 \le i \le d \end{aligned} \tag{5}$$

Q_l^H and Q_L are left Π-real matrix which is defined as matrices $Q \in \mathbb{C}^{L \times L}$ satisfying $\Pi_M \overline{Q} = Q$ [21, 24]. The unitary matrix

$$Q_{2q+1} = \frac{1}{\sqrt{2}} \begin{bmatrix} I_q & 0 & jI_q \\ 0 & \sqrt{2} & 0 \\ \Pi_q & 0 & -j\Pi_q \end{bmatrix}, \tag{6}$$

for example, is left Π-real of odd order. The unitary left Π-real matrix of size $2q \times 2q$ is obtain from (6) by dropping its center row and center column.

In the first step of UESPRIT [25, 26], forward-backward averaging is achieved by transforming the complex-valued data matrix X into real-valued matrix, Viz.

$$T(X) = Q_L^H [\ X \quad \Pi_L \overline{X} \Pi_N \ ] Q_{2N} \in \Re^{L \times 2N}. \tag{7}$$

Its d dominant left singular vectors $E_s \in \Re^{L \times d}$ are determined by performing the real-valued SVD on $T(X)$. Without additive noise, E_s and D span the same d-dimensional subspace. Thus there must be a nonsingular matrix Γ of size $d \times d$ such that $D \approx E_s \Gamma$. Substituting this relationship into (4) yields real-valued invariance equations

$$K_1 E_s^{\Upsilon} \approx K_2 E_s \text{ where } \Upsilon = \Gamma \Omega \Gamma^{-1}. \tag{8}$$

The invariance Equation (8) can be solved via least square (LS), yielding real-valued matrix Υ.
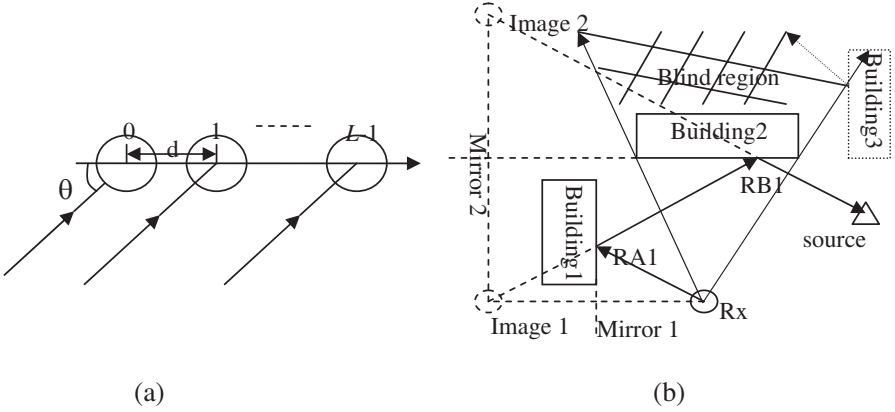
Figure 2. (a) Uniform linear array (ULA); (b) BRT principle and blind region.

The algorithm described above can easily be changed to R dimensional (R-D) case by substituting $a(\mu_i)$ with $a(\mu_i^1, \ldots, \mu_i^R) = a(\mu_i^R) \otimes a(\mu_i^{R-1}), \ldots, \otimes a(\mu_i^1)$ in (2b). $\otimes$ denotes Kronecker product. In the R-D case, the automatic pairing of the Eigen values of the R real-valued matrices $\Upsilon_1, \ldots, \Upsilon_R$ can be obtained by Simultaneous Schur Decomposition (SSD) [22, 25, 26].

3. THE LOCATION SCHEME

Step one: Estimate the DoA and TDoA with UESPRIT

The receive antenna used is a uniform linear array (ULA), as shown in Fig. 2(a). Assuming that the transmitter emits M single-tone signals $e^{-j2\pi(f_0+m\Delta f)t}$ ($m = 0, \ldots, M - 1$) and the impinging wave fronts on the receiver are approximately planar. The received signal of the m-th tone on the l-th sensor of ULA reads

$$y_{l,m}(t) = \sum_{i=1}^{N} A_i e^{-j2\pi(f_0+m\Delta f)(t-\tau_i-\frac{dl\sin\theta_i}{c})} + n(t), \qquad (9)$$

where, l (from 0 to $L - 1$) denotes the index of antenna sensors of the ULA at Rx, N: The number of propagation paths that can be performed by using the modified MDL proposed in [23, 28], A_i: Path loss, f_0: Center frequency, Δf: Frequency gap, d: Sensors interval, θ_i: The i-th path arrival angle, τ_i: The i-th path delay, and $n(t)$: The additive white Gaussian noise. In the simulation $M \cdot \Delta f \cdot d \cdot L/c < 0.01$,

so (9) can be simplified to [27]

$$y_{l,m}(t) = \sum_{i=1}^{N} A_i e^{-j2\pi f_0(t-\tau_i)} e^{j2\pi m \Delta f \tau_i} e^{j2\pi f_0 \frac{dl\sin\theta_i}{c}} + n(t) \quad . \quad (10)$$
$$\mu_i^1 = 2\pi f_0 \frac{d\sin\theta_i}{c} \text{ and } \mu_i^2 = 2\pi \Delta f \tau_i$$

Here we sample one temporal snapshot of each tone, and then perform a smoothing technique to divide the frequency dimension into g snapshots (groups), each containing $M_s = M - g + 1$ frequency points. Consequently, the signal parameters $\widetilde{\tau}_N = [\widetilde{\tau}_1, \ldots, \widetilde{\tau}_N]^T$ and $\widetilde{\theta}_N = [\widetilde{\theta}_1, \ldots, \widetilde{\theta}_N]^T$ can be obtained using 2-D UESPRIT in (10).

Step Two: Locating the source using BRT

An SBR/image approach [29] is used in the BRT technique. With the estimated parameters sets $\widetilde{\tau}_N = [\widetilde{\tau}_1, \ldots, \widetilde{\tau}_N]^T$ and $\widetilde{\theta}_N = [\widetilde{\theta}_1, \ldots, \widetilde{\theta}_N]^T$ derived by UESPRIT, the arrival angles and the lengths of path which the signals have been traveled can be obtained. According to these angles, the Back Ray Tracing (BRT) emits signals from the receiver (Rx), as shown in Fig. 2(b). Then the propagating waves will move forward, hit all the surfaces of the buildings, and a number of points of intersection are obtained. The nearest intersection point (RA1) is the place where the wave is reflected. Then, image 1 is symmetrical with the Rx with respect to the surface (mirror 1) where the nearest intersection point is on. Consequently the direction of the reflection wave is the direction of the line connecting image1 and RA1. Subsequently image 2 and the second reflected direction can be found in the same way. The propagation wave will move until the lengths of the path reach the estimated ones. The stop position is the source location. The final estimated source location is determined by average of all the estimated locations corresponding to each path, as shown in Equation (11),

$$\overline{x} = \frac{1}{N} \sum_{i=1}^{N_s} \widehat{x}_i \text{ and } \overline{y} = \frac{1}{N} \sum_{i=1}^{N_s} \widehat{y}_i. \quad (11)$$

$(\widehat{x}_i, \widehat{y}_i)$ is estimated locations, and $(\overline{x}, \overline{y})$ is the final estimated location.

4. ERROR ANALYSES OF THE ALGORITHM

According to the above discussion, the errors consist of two parts: The first one is caused by the finite accuracy of UESPRIT, e.g., the DoA and ToA errors, while the second one is the terrain data error compared with the real scene. Besides, there may be some blind region where the source can not be located.

4.1. Parameter Estimation Accuracy of UESPRIT

Here we will test the accuracy of the UESPRIT algorithm. We duplicate the simulation example in [22], which was conducted with 4 wave fronts, a 2×2 URA and 10 temporal snapshots. The 4 vectors need being estimated are: $\mu_1 = \pi[0.05 \ -0.5 \ 0.8]^T$, $\mu_2 = \pi[0.5 \ 0.5 \ 0.8]^T$, $\mu_3 = \pi[0.5 \ 0.5 \ 0.2]^T$, and $\mu_4 = \pi[0.0 \ 0.2 \ 0.2]^T$. Fig. 4(a) gives the root mean squared error (RMSE) of the simulation results by our UESPRIT program. Our results of RMSE are similar with that in Fig. 4 of [22] in the order of the magnitude.

Because the estimation accuracy is related with the size of antenna array L and the number of snapshots g (where $g = M - M_s + 1$), we need to test the estimation accuracy of our simulation model. In this paper, we set the parameters of our model to be $f_0 = 2$ GHz, $\Delta f = 1 \times 10^4$ GHz, $L = 10$, $M_s = 10$, $M = 300$, and $d = 0.5\lambda$, where $\lambda = c/f_0$ and $c = 3 \times e^8$ m/s. Four wave fronts arrive at the receiving antenna array from the source with different arrival angle and path length, viz. $(-\pi/6, 120$ m), $(-\pi/3, 60$ m), $(\pi/4, 200$ m) and $(\pi/9, 390$ m). One thousand realizations of the estimation accuracy of UESPRIT versus SNR are computed. Fig. 4(a) shows the RMSE of μ_i^1 and μ_i^2. To achieve intuitive observation, we separate the RMSE into two part: RMSE of DOA and RMSE of path length. Fig. 4(b) implies that the estimation accuracy of DOA is below 0.55 degree and that of path length is below 6 meters. All these estimations satisfy the requirements for the high resolution localization.

4.2. Localization Errors Caused by UESPRIT

If the signal paths hit around the corner of the building, as shown in Fig. 3, the errors caused by UESPRIT will be extremely significant. In

                    (a)   (b)
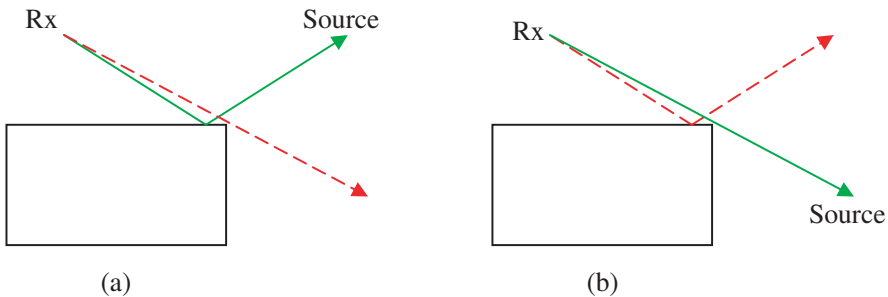
Figure 3. Error models (solid line: real path, dash line: estimated path.
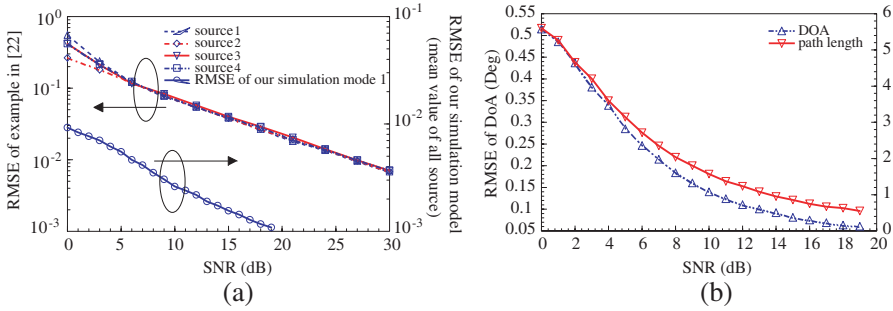
Figure 4. Estimation accuracy of UESPRIT (1000 realizations) (a) RMSE of the simulation example in [22] and our simulation model. (b) RMSE of DoA and path length of our simulation model.

these situations (Fig. 3), the estimated position obtained from BRT will be far away from the real source position. The terrain data error can also cause this problem. In order to eliminate this error, the estimated positions must be selected. Here we propose a valid range selection scheme for the judgment of the validity of the estimated position data, using Equation (12)

$$
\left\{
\begin{array}{ll}
\Delta_{i,j} = \sqrt{(\widehat{x}_i - \widehat{x}_j)^2 + (\widehat{y}_i - \widehat{y}_j)^2} & i \neq j, i, j = 1, \ldots, N \\
\Delta_{i,J} = \sqrt{(\widehat{x}_i - \widehat{x}_J)^2 + (\widehat{y}_i - \widehat{y}_J)^2} & i \neq J, i = 1, \ldots, N \\
\Delta_{i,J} < \Delta r
\end{array}
\right. , \quad (12)
$$

where $(\widehat{x}_i, \widehat{y}_i)$ and $(\widehat{x}_j, \widehat{y}_j)$ are the estimated localizations, $(\widehat{x}_J, \widehat{y}_J)$ is one of the two closest estimated localizations, N denotes the number of paths considered, $\Delta_{i,j}$ denotes the distance between two estimated localizations, $\Delta_{i,J}$ denotes the distance between the estimated localization and the center of the valid range, Δr denotes the threshold used to determine whether the result is reliable. Through out this paper Δr is chosen as $3\,\mathrm{m}$. In the selection procedure, we first calculate the distance between any two estimated localizations $\Delta_{i,j}$, and then set one of the two estimated localizations that are nearest to each other as the center of our selection range, viz. $(\widehat{x}_J, \widehat{y}_J)$. Subsequently, an estimated localization is valid if the distance from it to the center of the selection range is less than Δr. After eliminating the invalid estimated positions, the average of those valid estimated positions will be made, which is the ultimately estimated source location, as in Equation (11).
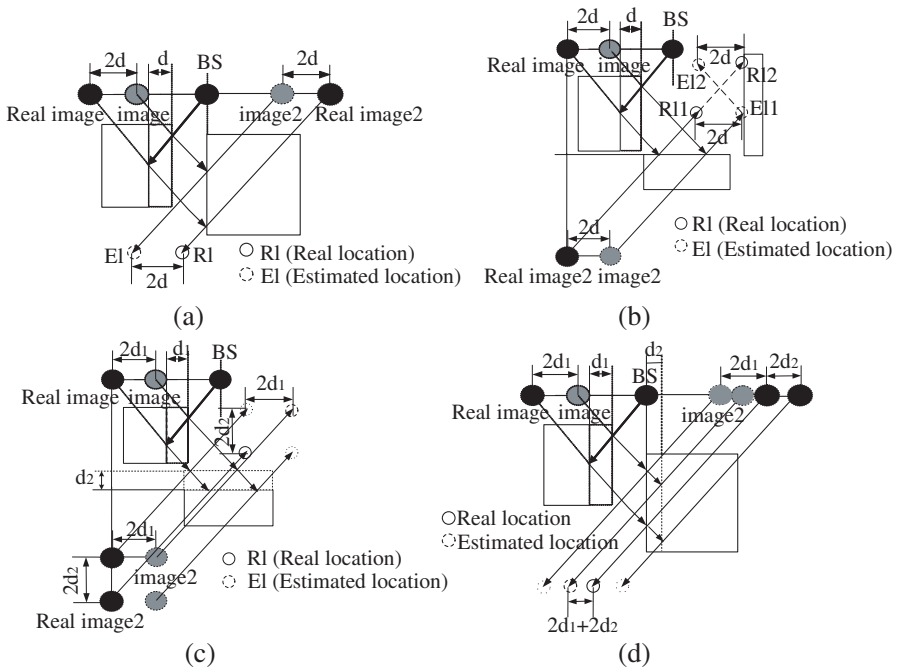
Figure 5. Error caused by terrain inaccuracy (a) error caused by one wall. (b) error caused by one wall (when estimated path is reflected one more time than real one) (c) error caused by two perpendicular walls (d) error caused by two parallel walls.

4.3. Localization Errors Caused by Terrain Inaccuracy

The estimated accuracy is also related to the resolution of terrain data. In the second step of our position method the BRT recovers the signals propagation paths with the terrain data and the signals parameters obtained from step one. Usually, the geometry data of the terrain is inaccurate. In the following, we will analyze how the terrain data inaccuracy influents the estimated results in four cases and then give an effective measure to minimize these errors.

Case (a): If one of the walls is not in the real place, the distance from the real place is d, then the estimated location is $2d$ from the real location, as shown in Fig. 5(a).

Case (b): In Fig. 5(b) the estimated path is reflected one more time than the real propagation path, it is easy to find out that the estimated error is less than $2d$.

Case (c): If there are two walls perpendicular with each other, which are d_1 and d_2 from the real positions respectively, as shown in Fig. 5(c), the distance between the estimated location and real location is

$$\Delta d = \sqrt{(2d_1)^2 + (2d_2)^2}. \tag{13}$$

Case (d): If two parallel walls as shown Fig. 5(d) are d_1 and d_2 from the real positions respectively, the distance between the estimated location and real location is

$$\Delta d = 2d_1 + 2d_2. \tag{14}$$

So the estimated error caused by the terrain data error can be summarized as

$$\Delta d \le \sqrt{\left(\sum_{i=1}^{N_x} 2d_i\right)^2 + \left(\sum_{j=1}^{N_y} 2d_j\right)^2} \le \sum_{i=1}^{N_x+N_y} 2|d_i|. \tag{15}$$

N_x and N_y denote the numbers of error walls parallel with x axis and y axis respectively.

According to (15), the estimated error increases if the number of signal reflections increases. From the statistical point of view, the number of inaccurate walls that the signal has passed is proportional to the path length. So, here we introduce a path length weighting factor to each valid estimated positions, and determine the final estimated position by the weighted plus of all the valid estimated positions as

$$\omega_i = \frac{1}{pl_i^2} \Big/ \sum_{i=1}^{N_s} \frac{1}{pl_i^2}$$
$$\overline{x} = \sum_{i=1}^{N_s} \omega_i \widehat{x}_i \text{ and } \overline{y} = \sum_{i=1}^{N_s} \omega_i \widehat{y}_i \tag{16}$$

where $(\widehat{x}_i, \widehat{y}_i)$ and $(\overline{x}, \overline{y})$ are the estimated localizations and the estimated result respectively, ω_i is the weighting factor, pl_i is the ith path length, and N_s denotes the number of the valid results, which is selected according to Equation (12).

4.4. Blind Region

One problem of the BRT technique is that the diffraction path can not be recovered. Hence, at least one reflection path or LOS path is needed if the source can be accurately located. In Fig. 2(b), there is not any reflection or direction path in the blind region, only the diffraction path can reach there. In order to avoid the blind region, we can build a reflector (building 3) or more Rx to introduce the reflection path.

5. NUMERICAL RESULTS

Six simulations examples are carried out in this paper. In these simulations the parameters are set to be $f_0 = 2.4\,\text{GHz}$, $\Delta f = 1 \times 10^4\,\text{GHz}$, $L = 10$, $M_\text{s} = 10$ and $d = 0.5\lambda$ ($\lambda = c/f_0$, $c = 3 \times e^8\,\text{m/s}$). Three terrain data are employed, as shown in Fig. 6 and Fig. 9.

Simulation 1. The receiver was fixed on $(10, 30)$, while the transmitter moves along the dash line with a step of 0.5 m, as shown in Fig. 6(a). A total of 120 positions is sampled and 22 realizations have been carried out. In each transmit location the position estimation is carried out in all values of SNR with different numbers of frequency points, viz., SNR from 0 to 20 dB and $M = 300$, 100, and 60. The relation between the average estimation error and SNR was shown in
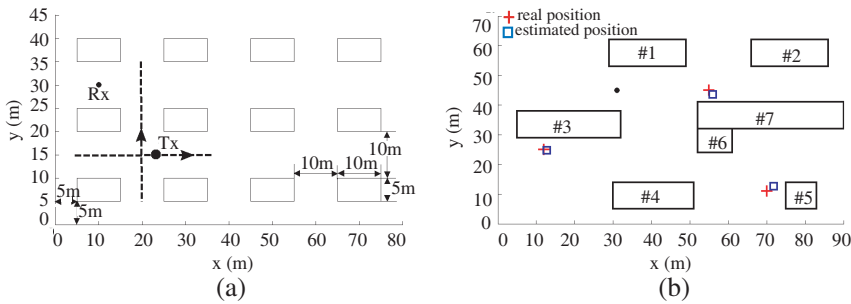
Figure 6. (a) The simulation scenery in [30]; (b) multisource position in the scenery similar to that in [31].
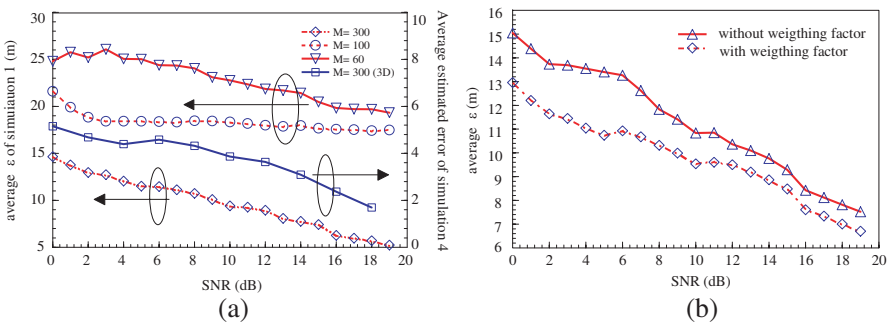
Figure 7. (a) The estimated error (22 realizations) of simulation 1 and 3D localization accuracy of Simulation 4. (b) The position estimation under terrain errors (22 realizations) of simulation 2.

Fig. 7(a). The $\overline{\varepsilon}$ is defined as $\overline{\varepsilon} = \sum_{i=1}^{n} \sqrt{(\overline{x}_i - x_i)^2 + (\overline{y}_i - y_i)^2}/n$, where $(\overline{x}_i, \overline{y}_i)$ and (x_i, y_i) denote the estimated position and real position respectively, n denotes the number of the positions. The simulation results imply that more frequency point we use, more snapshots we have, and higher the estimation accuracy we can obtain.

Simulation 2. In this simulation the frequency points is set as $M = 300$ and errors of the lengths and widths of the buildings are assumed to be Gaussian distributed with zero-mean and variance $\sigma = 0.707$ m. Here, the transmitter also moves along the dash line as in simulation 1, the estimated results using average method and the weighting factor are both shown in the Fig. 7(b). 22 realizations have been carried out. With the help of the weighting factor the estimated accuracy is improved, especially in low SNR condition.

Simulation 3. In this simulation, three different sources ask for locations simultaneously. Here we assume SNR $= 20$ dB and $M = 300$. The receiving antenna array is fixed in $(31, 45)$, and three sources locate in $(55, 45)$, $(12, 25)$ and $(70, 11)$ respectively. All the dominant paths parameters, viz. DoA and ToA corresponding to the three sources, can be obtained by UESPRIT. Then with these parameters three positions can be found after performing BRT and the selection criteria. The estimated position is $(55.924, 43.478)$, $(12.768, 24.737)$ and $(71.845, 12.561)$, as shown in Fig. 6(b). Table 2 contains the specific parameters of the buildings that are utilized in this simulation. The multi-source localization does not always work precisely. Sometimes, the number of estimated source positions is bigger than the real number. However, it is useful for some emergency cases, e.g., life detections.

The extension of this method to three dimension cases is straightforward. In the following, three 3D simulations are conducted. In order to estimate the elevation angle we should add one dimension to the antenna array, viz., a 10×10 elements uniform rectangular array (URA) instead of the 10 elements ULA are employed now. The frequency points are 300.

Table 2. Parameters of the buildings in Figure 6(b) (unit: m).

Building	#1	#2	#3	#4	#5	#6	#7
Centroid	(39 57.5)	(76 57.5)	(18.5 33.5)	(40.5 9.5)	(79 9.5)	(56.5 28)	(71 36.5)
Length	20	20	27	21	8	9	38
Width	9	9	9	9	9	8	9

	Position	Estimated position	Δ
Tx1	(8 52 1.6)	(8.7 52 2.8)	1.39
Tx2	(20 20 1.8)	(22.9 20.4 1.3)	2.97
Tx3	(60 10 1.6)	(60.3 9.8 2)	0.54
Tx4	(43 32 1.7)	(39.7 32 0.7)	3.45
Tx5	(60 58 2)	(62.6 57.9 2.5)	2.65

(a)   (b)
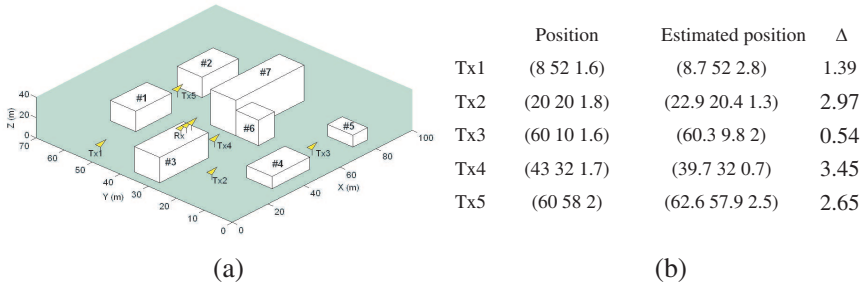
Figure 8. (a) 3D terrain data of simulation 5 (height of buildings: #1 and #2: 20 m; #3 and #6: 25 m; #4 and #5: 12 m; #7: 35 m), (b) Estimated results of simulation 5 (SNR = 20 dB).

(a)   (b)

(c)
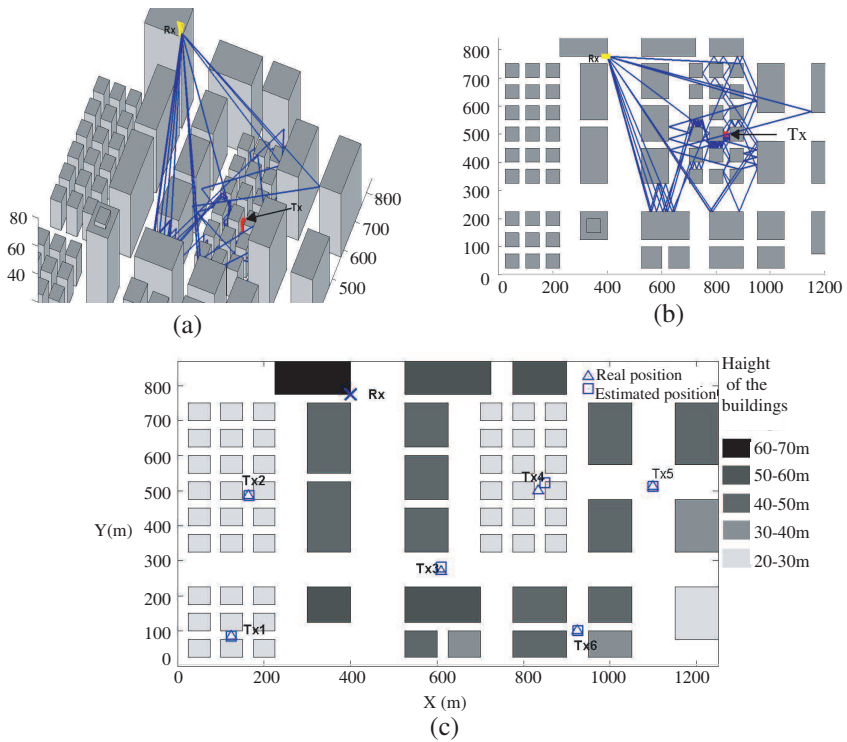
Figure 9. (a) Propagation paths from Tx to Rx in 3D terrain, (b) planform of paths from Tx to Rx, (c) top view of the 3D terrain and the estimated results.

Simulation 4. We change 2D terrain data shown in Fig. 6(a) to 3D by adding a height to each building. the height of all the buildings is 24 meters. We assume a source with 1.6 meters tall moves on the street as simulation 1 and the receiving antenna array is fixed on the top of the building $(10, 35, 28)$, which is 4 meters higher than the building. There are more LoS paths in this simulation than in simulation 1, so that the estimated accuracy is a little better than 2D case, as shown in Fig. 7(a).

Simulation 5. The terrain data is shown in Fig. 8(a) and the top view of this terrain is shown in Fig. 6(b). In this simulation, the receive antenna array is fixed on $(30, 33, 28)$, which is 3 meters over the top of #3 building. We test this method in five typical positions and the estimated results are listed in the Fig. 8(b). In Fig. 8(b), Δ denotes the distance between the true position and the estimated one. We can see that the estimated positions are extremely close to the real positions.

Simulation 6. In order to further test our position method, a more complicated and realistic terrain is considered in this simulation, as shown in Fig. 9. The receiving antenna array is fixed on the top of the highest building $(400\ 775\ 68)$, (3 meters higher than the building). Six position estimations in different district are conducted, as shown in Fig. 9(c). The propagation environment is very complex in this terrain, viz. propagation paths from Tx4 to Rx, as shown in Figs. 9(a) and (b). It is more difficult to pinpoint the source position. The estimated results of this simulation is listed Table 3, and it also can be found in Fig. 9(c). Usually, the elevation angles of most paths are close to each other. That makes a little difficulty to precisely estimate the elevation angle. As a result the estimated error in z-direction is

Table 3. Estimated results of simulation 6.

SNR=20 dB	Position	Estimated position	Δ
Tx1	(125 85 1.8)	(124.7 84.2 3.8)	2.2
Tx2	(165 485 1.7)	(165.6 485.5 4.5)	2.9
Tx3	(600 300 1.7)	(610.6 281.5 10.5)	23.1
Tx4	(835 500 1.7)	(850.1 522.8 5.8)	27.7
Tx5	(1100 512 1.6)	(1100.3 511.9 6.8)	5.2
Tx6	(925 100 1.8)	(925.6 99.6 20.4)	18.6

higher than that in x-y direction.

Simulation 7. In our paper, the diffraction paths are not considered in our simulation model. We take the diffraction paths as a noise. According to the uniform geometrical theory of diffraction, the diffraction coefficients are very small compared with the reflection coefficients. To illustrate this, here, we give an example. A source is assumed to be located at (30 15 1.5) of the terrain data in simulation 4, and the receiver is fixed on (15 35 28). Four reflection paths and four dominant diffraction paths arrive at the receiver, as shown in Table 4. We can see that the power of reflection paths and the diffraction paths (normalized by the maximum path power) are not in the same order of magnitude. The final estimated position is (30.59 14.68 1.54). This demonstrates that when there are reflection paths between the source and the base station, the effect of the diffractions on the source localization can be ignored. If the source is in blind region, viz., no reflection path exists, our method will apparently fail. Nevertheless, the potential application value of our methods is significant, because in the future wireless communications (Beyond 3rd Generation and the 4th Generation) the coverage area of a base station will become smaller and hence the probability of encountering the blind region in source localization also will be reduced.

Before the end of this section, we also give a brief summary of the CPU time used in these six simulations. For 2D cases, the computation times of the UESPRIT and BRT program for position once are about 0.19 seconds and 58.3 μs respectively (for both single source and multi-source cases). For 3D cases, the computation times of the UESPRIT and BRT program for position once are about 13.8 seconds and 58.3 μs, respectively. All these simulations are carried out in a 3.0 GHz CPU. This demonstrates the efficiency of our localization algorithm.

Table 4. Parameters of the received signals from a source located at (30 15 1.5) (SNR = 20 dB).

	Reflection paths				Dominant diffraction paths			
	Path 1	Path 2	Path 3	Path 4	Path 5	Path 6	Path 7	Path 8
θ_i	5.176	5.176	5.865	5.865	5.82	5.3	4.712	5.3
φ_i	2.239	2.292	2.064	2.111	2.064	2.383	2.328	2.235
$\tau_i \cdot c$	42.746	44.668	55.922	57.404	55.959	36.499	38.572	42.981
power	1	0.77	0.93	0.79	$1.23e-02$	$0.89e-03$	$1.31e-03$	$2.62e-03$

6. CONCLUSION

In this paper, we proposed a novel source localization scheme based on the UESPRIT with BRT and the city electronic maps. This method can estimate both the LOS and NLOS source accurately. The main points of this scheme are summarized as follows.

- UESPRIT is employed to estimate the arrival angles and delays of the rays radiated from the source. Based on the obtained information, the source position can be obtained according to the BRT program and the city electronic map.

- A valid range selection criterion is devised for the judgment of the validity of the estimated position data.

- This method uses a path length weighting factor to determine the final estimated position.

Error analysis shows that the estimated accuracy has correlative relationship with the estimated accuracy of UESPRIT and the resolution of the terrain data. A selection criterion and a path length weighting factor weaken those influences. Our simulation results demonstrate that the estimated accuracy is high in the urban environment with the help of the selection criterion and the path length weighting factor. Moreover, this method can also be applied to 3D environments.

ACKNOWLEDGMENT

REFERENCES

1. Tayebi, A., J. Gómez, F. S. Saez De Adana, and O. Gutierrez, "The application of ray-tracing to mobile localization using the direction of arrival and received signal strength in multipath indoor environments," *Progress In Electromagnetic Research*, PIER 91, 1–15, 2009.

2. Soliman, M. S., T. Morimoto, and Z. I. Kawasaki, "Three-dimensional localization system for impulsive noise sources using ultra-wideband digital interferometer technique," *Journal of Electromagnetic Waves and Applications*, Vol. 20, No. 4, 515–530, 2006.

3. Soliman, M. S., A. Hirata, T. Morimoto, and Z. I. Kawasaki, "Numerical and experimental study on three-dimensional localization for ultra-wideband impulsive noise sources," *Journal of Electromagnetic Waves and Applications*, Vol. 19, No. 2, 175–187, 2005.

4. Liew, S. C., K. G. Tan, and C. P. Tan, "Non-taylor series based positioning method for hybrid GPS/cellphone system," *Journal of Electromagnetic Waves and Applications*, Vol. 20, No. 6, 717–729, 2006.

5. Liew, S. C., K. G. Tan, and T. S. Lim, "Investigation of direct A-GPS positioning for hybrid E-OTD/GNSS," *Journal of Electromagnetic Waves and Applications*, Vol. 20, No. 1, 79–87, 2006.

6. Chueng, K. W., H. C. So, W.-K. Ma, and Y. T. Chan, "Least square algorithms for time-of-arrival based mobile location," *IEEE Trans. Signal Processing*, Vol. 52, 1121–1128, Apr. 2004.

7. Wang, X., Z. X. Wang, and B. O. Dea, "A TOA based location algorithm reducing the errors due to Nom-Line-of-Sight (NLOS) propagation," *IEEE Trans. Veh. Tech.*, Vol. 52, 112–116, 2003.

8. Caffery, J. J., *Wireless Location in CDMA Cellular Radio Systems*, KAP, 1999.

9. Landesa, L., I. T. Castro, J. M. Taboada, and F. Obelleiro, "Bias of the maximum likelihood DOA estimation from inaccurate knowledge of the antenna array response," *Journal of Electromagnetic Waves and Applications*, Vol. 21, No. 9, 1205–1217, 2007.

10. Harabi, F., H. Changuel, and A. Gharsallah, "Direction of arrival estimation method using a 2-L shape arrays antenna," *Progress In Electromagnetics Research*, PIER 69, 145–160, 2007.

11. Deng, P. and P. Z. Fan, "An AOA assisted TOA position system," *ICCT 2000 Proceedings*, 1501–1504, Beijing, Aug. 2000.

12. Cong, L. and W. H. Zhuang, "Hybrid TDOA/AOA mobile users location for wideband CDMA cellular system," *IEEE Trans. Wireless Commun.*, Vol. 1, 439–447, Jul. 2002.

13. Cong, L. and W. H. Zhuang, "Non-line-sight error mitigation in mobile location," *IEEE Trans. Wireless Commun.*, Vol. 4, 560–572, Mar. 2005.

14. Chen, P. C., "A non-line-of-sight error mitigation algorithm in location estimation," *Proc. IEEE Wireless Communications Networking Conf.*, Vol. 1, 316–320, 1999.

15. Chan, Y. T., W. Y. Tsui, H. C. So, and P. C. Ching, "Time-of-arrival based localization under NLOS conditions," *IEEE Trans.*

Veh. Tech., Vol. 55, 17–24, Jan. 2006.

16. Algeier, V., B. Demissie, W. Koch, and R. Thomae, "Blind localization of 3G mobile terminals in multipath scenarios," *Proceedings of the 3rd Workshop on Position and Communication*, 219–226, 2006.

17. Kikuchi, S., A. Sano, H. Tsuji, and R. Miura, "A novel approach to mobile-terminal positioning using signal array antenna in urban environments," *Proc. VTC IEEE*, 1010–1014, 2003,

18. Seow, C. K. and S. Y. Tan, "Localization of omni-directional mobile device in multipath environments," *Progress In Electromagnetic Research*, PIER 85, 323–348, 2008.

19. Teh, C. H., F. Kung, and H. T. Chuah, "A path-corrected wall model for ray-tracing propagation modeling," *Journal of Electromagnetic Waves and Application*, Vol. 20, No. 2, 207–214, 2006.

20. Jin, K.-S., T. I. Suh, S. H. Suk, B. C. Kim, and H. T. Kim, "Fast ray tracing using a space-division algorithm for RCS prediction," *Journal of Electromagnetic Waves and Applications*, Vol. 20, No. 1, 119–126, 2006.

21. Haardt, M. and J. A. Nossek, "Unitary ESPRIT: How to obtain increased estimation accuracy with a reduced computational burden," *IEEE Trans. Signal Processing*, Vol. 43, 1232–1242, May 1995.

22. Haardt, M. and J. A. Nossek, "Simultaneous schur decomposition of several nonsymmetric matrices to achieve automatic pairing in multidimensional harmonic retrieval Problems," *IEEE Trans. Signal Processing*, Vol. 44, 161–169, Jan. 1998.

23. Xu, G., H. R. Richard, and T. Kailath, "Detection of number of sources via exploitation of centro-symmetry Property," *IEEE Trans. Signal Processing*, Vol. 42, 102–112, Jan. 1994.

24. Lee, A., "Centrohermitian and skew-centrohermitian matrices," *Linear Algebra Applicat.*, Vol. 48, 198–212, 1994.

25. Zoltowski, M. D., M. Haardt, and C. P. Mathews, "Closed-form 2D angle estimation with rectangle arrays in element space or beamspace via unitary ESPRIT," *IEEE Trans. Signal Proceeding*, Vol. 44, 316–329, Feb. 1996.

26. Haardt, M., *Efficient One-, Two- and Multidimensional High-Resolution Array Signal Proceeding*, J. A. Nossek, Ed. Aachen, Shaker Verlag, Germany, 1996.

27. Zwick, T., D. Hampicke, A. Richter, G. Sommerkorn, R. Thoma, and W. Wisebeck, "A novel antenna concept for double-directional

channel measurements," *IEEE Trans. Veh. Tech.*, Vol. 53, 527–537, Mar. 2004.

28. Wax, M. and T. Kailath, "Detection of signal by information theoretic criteria," *IEEE Trans. on Acoustics, Speech, and Signal Processing*, Vol. 33, 387–392, Apr. 1985.

29. Chen, S. H. and S. K. Jeng, "An SBR/image approach for radio wave propagation in indoor environments with metallic furniture," *IEEE Trans. Antennas Propagrat.*, Vol. 45, No. 1, 98–106, Jan. 1997.

30. Har, D., H. H. Xia, and H. L. Bertoni, "Path-loss prediction model for microcells," *IEEE Trans. Veh. Tech.*, Vol. 18, No. 5, 1453–1462, Sep. 1999.

31. Liang, G. and H. L. Bertoni, "A new approach to 3-D ray tracing for propagation prediction in cities," *IEEE Trans. Antennas Propagrat.*, Vol. 46, No. 6, 853–863, Jun. 1998.

32. Ni, H., G. Ren, and Y. Chang, "A TDOA location scheme in OFDM based WMANs," *IEEE Transactions on Consumer Electronics*, Vol. 54, No. 3, 1017–1021, Aug. 2008.

33. Kaemarungsi, K. and P. Krishnamurthy, "Modeling of indoor positioning systems based on location fingerprinting," *Proceedings of the 23th Annual Joint Conference of the IEEE Computer and Communications Societies*, Vol. 2, 1012–1022, Hong Kong, Mar. 2004.

34. Ahonen, S. and P. Eskelinen, "Mobile terminal location for UMTS," *IEEE Aerospace and Electronic Systems Magazine*, Vol. 18, No. 2, 23–27, 2003.

35. Proakis, J. G. and M. Salehi, *Communication Systems Engineering*, 2nd edition, Publishing House of Electronics Industry, Beijing, 2007.